

Stabilization of space–time laser instability through the finite transverse extension of pumping

D. Amroun-Aliane, Hervé Leblond, Marc Brunel, Christophe Letellier, François Sanchez

▶ **To cite this version:**

D. Amroun-Aliane, Hervé Leblond, Marc Brunel, Christophe Letellier, François Sanchez. Stabilization of space–time laser instability through the finite transverse extension of pumping. Journal of Optics A: Pure and Applied Optics, 2008, 10 (9), pp.095101. 10.1088/1464-4258/10/9/095101 . hal-03436298

HAL Id: hal-03436298

https://univ-angers.hal.science/hal-03436298

Submitted on 19 Nov 2021

HAL is a multi-disciplinary open access archive for the deposit and dissemination of scientific research documents, whether they are published or not. The documents may come from teaching and research institutions in France or abroad, or from public or private research centers.

L'archive ouverte pluridisciplinaire **HAL**, est destinée au dépôt et à la diffusion de documents scientifiques de niveau recherche, publiés ou non, émanant des établissements d'enseignement et de recherche français ou étrangers, des laboratoires publics ou privés.

J. Opt. A: Pure Appl. Opt. **10** (2008) 095101 (7pp) doi:10.1088/1464-4258/10/9/095101

Stabilization of space–time laser instability through the finite transverse extension of pumping

D Amroun[1], H Leblond[2], M Brunel[3], C Letellier[3] and F Sanchez[2]

[1] Laboratoire d'Electronique Quantique, Université des Sciences et de la Technologie d'Alger, BP 32, El Alia Bab Ezzouar, 16111 Alger, Algeria
[2] Laboratoire POMA, FRE 2988, Université d'Angers, 2 Bd Lavoisier, 49045 Angers cedex 01, France
[3] CORIA UMR 6614-Université de Rouen, Av. de l'Université, BP 12, 76801 Saint-Etienne du Rouvray cedex, France

Received 29 April 2008, accepted for publication 17 July 2008
Published 19 August 2008
Online at stacks.iop.org/JOptA/10/095101

Abstract
We investigate the space–time dynamics of a homogeneously broadened single-mode laser when diffraction is taken into account. It is well known that such a laser displays instability when pumping reaches the second laser threshold. We show that the laser dynamics can be stabilized by pumping in a domain of finite width. The analysis of stationary solutions to the Maxwell–Bloch equations (evanescent waves, travelling waves, localized solutions) allows the stabilization mechanism to be explained.

Keywords: laser instability, stabilization, Maxwell–Bloch equations

(Some figures in this article are in colour only in the electronic version)

1. Introduction

Laser dynamics has attracted much interest in the last decades. Since the pioneering work of Haken, who established the analogy between the dynamics of a flow and the dynamics of a homogeneously broadened single-mode laser [1], many studies have been carried out and a wide range of dynamic laser behaviours has been observed and predicted. However, the actual observation of some of the predicted dynamics can be very difficult, or even impossible. We can, for example, consider the case where the parameters do not really describe existing lasers. This is often the case for class-C lasers, which require decay times that are comparable for the photon in the cavity, the population inversion and the polarization. Predicted dynamics thus appear just as fascinating models, except for the NH_3 class-C laser described by Tang *et al* [2, 3]. In many cases, other effects can occur that perturb the dynamics so that the prediction cannot be observed. One of the first examples was given by Lugiato and Milani [4, 5]. They showed that if a fixed Gaussian laser mode transverse intensity distribution was assumed, there were no longer any 'bad-cavity' or 'good-cavity' single-mode laser instabilities in a homogeneously broadened laser. More recently, it has been demonstrated that spatial inhomogeneities, such as the spatial dependence of a control parameter, could prevent pattern stability in optical systems [6, 7]. In the present paper, we are interested in the space–time dynamics of a homogeneously broadened single-mode laser when diffraction is taken into account. Previous studies have demonstrated that under homogeneous pumping, instability can be observed, depending on the pumping parameter and the detuning [8–11]. In this paper we show that this instability can be eliminated when a localized (super-Gaussian or top-hat) transverse pumping distribution is considered. The same result is obtained when a Gaussian or stiff-edge profile is assumed. The stabilization mechanism is explained in terms of evanescent waves created on the edges of the pumping region.

The paper is organized as follows. The end of the introduction will present a brief summary of the laser system under study. Section 2 will then present numerical evidence of the stabilization process under a non-uniform transverse pumping profile. To interpret the results, it will be necessary to determine different classes of solution, such as evanescent

 © 2008 IOP Publishing Ltd Printed in the UK

wave solutions: this will be done in section 3. Finally, section 4 will detail the stabilization mechanism.

Our analysis starts with the Maxwell–Bloch equations for a large-aspect-ratio homogeneously broadened two-level laser with plane and parallel mirrors in the rotating wave, slowly varying amplitude, and single-longitudinal-mode approximations. They are written as [8, 11]

$$\partial_t e = -\sigma(e - p) + \mathrm{i}A\partial_x^2 e, \tag{1}$$

$$\partial_t p = -(1 - \mathrm{i}\delta)p + ed, \tag{2}$$

$$\partial_t d = -\gamma\left(d - r + \tfrac{1}{2}\left(ep^* + e^* p\right)\right), \tag{3}$$

where e, p, and d are normalized expressions of the electric field, macroscopic polarization, and population inversion, respectively. $\gamma = \gamma_\parallel/\gamma_\perp$ and $\sigma = \gamma_\ell/2\gamma_\perp$, where $\gamma_\perp$, $\gamma_\parallel$, and γ_ℓ are decay rates of the polarization, population inversion, and optical intensity, respectively. Time is normalized versus the coherence lifetime; $\delta = (\omega - \omega_\mathrm{a})/\gamma_\perp$ is the detuning of the field frequency ω from the atomic transition frequency ω_a. A is the diffraction parameter. Parameter r represents the pumping. The partial differential operator $\partial/\partial t$ is denoted by ∂_t, and so on. The trivial solution is the off-state ($e = p = 0, d = r$). Above the lasing threshold, the system (1–3) admits a travelling wave solution for negative detuning or a homogeneous state for positive detuning [8]. The travelling wave solution can be expressed by

$$e = \overline{e}\, e^{\mathrm{i}(\Omega t + Kx)}, \tag{4}$$

$$p = \left[1 + \frac{\mathrm{i}}{\sigma}\left(\Omega + AK^2\right)\right]\overline{e}\, e^{\mathrm{i}(\Omega t + Kx)}, \tag{5}$$

$$d = r - |\overline{e}|^2, \tag{6}$$

with the fixed amplitude

$$|\overline{e}|^2 = r - 1 - (\Omega - \delta)^2, \tag{7}$$

and the dispersion relation

$$\Omega = \frac{\delta\sigma - AK^2}{1 + \sigma}. \tag{8}$$

Avoid any confusion between the frequency and wavenumber Ω and K of the envelope, and the optical frequency and wavenumber. K is a transverse wavenumber, small with respect to the optical wavenumber of the laser radiation, and Ω is a small frequency shift linked to this transverse component. Above the first laser threshold the laser selects the wavenumber with the lowest lasing threshold, which is $K = \sqrt{-\delta/A}$ for negative detunings and $K = 0$ for positive detunings [8, 11].

A linear stability analysis of these solutions can then be performed, leading to the determination of the second laser threshold (instability of the stationary state). The resulting stability diagram in the detuning δ and pumping parameter r plane (figure 1) reveals different instability domains [8, 11]. In particular, for positive detuning and a relatively low pumping parameter (2.55 times the first laser threshold that is roughly equal to 10.0), a very specific intermittent behaviour is observed [11]: the evolution of the laser intensity $I(x = 0, \tau) = |e(x = 0, \tau)|^2$ versus τ reveals time intervals of nearly constant intensity, interrupted by bursts of large amplitude oscillations (these computations, as well as the ones below, have been performed for the values of parameters $\delta = 3$ and $r = 25$. These values are marked on figure 1 by P). During each of these intervals, the dynamics is very close to a sinusoidal evolution of the electric field. The time evolution of the spatial Fourier spectrum $|\hat{e}(K, \tau)|$ further reveals that each nearly sinusoidal field evolution is associated with a unique wavevector K. Thus, each interval corresponds to a specific transverse travelling wave. This very uncommon behaviour is an intermittency structured around a few periodic orbits, always visited in a given order.

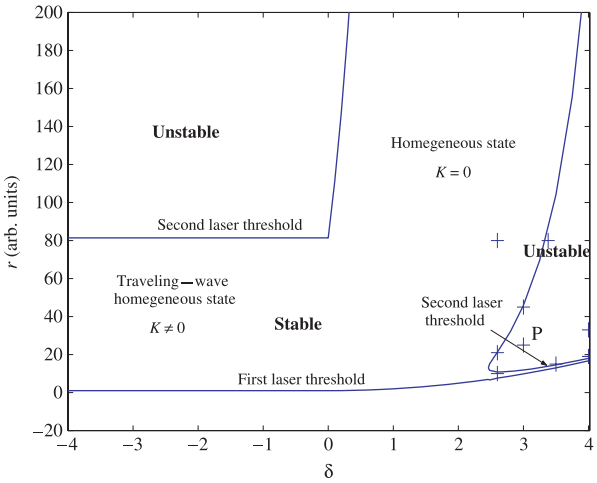


Figure 1. Stability diagram in the plane (δ, r). The point P indicates the values of δ and r used in the evolution computations. The crosses indicate the values for which the stability of the stationary state has been established. The other parameters are $\sigma = 0.01$, $\gamma = 0.2$, $A = 0.05$.

2. Numerical evidence for stabilization

Let us consider here an inhomogeneous (a non-uniform) pumping profile that limits the transverse expansion of the beam, as occurs in practice. We used both a super-Gaussian profile $r(x) = r_0 e^{-\rho^2 x^6}$, with $r_0 = 25$ and $\rho = 0.054$, which corresponds to a width $2x_m$ of the pumped region with $x_m = 2.5$, and a top-hat profile with the same width $2x_m = 5$ and level $r_0 = 25$ (see the dotted–dashed lines in figure 2). Other parameter values are $\sigma = 0.01$, $\gamma = 0.2$, $A = 0.05$ and $\delta = 3$. For uniform pumping, these values of r and δ (point P on figure 1) correspond to an unstable regime, above the second laser threshold. However, after a transient regime, the laser intensity reaches a constant value for both the localized pumping distributions considered here. Figure 2 shows the final transverse profile of the amplitude of the emitted wave field, which is stationary (solid lines), and a sech-square fit of this profile (dashed lines). The stability is proved by pursuing the computation of the evolution until $t = 10^4$, without any change in the profile. The transverse profile of the field amplitude appears to be roughly sech-square shaped, and vanishes in the regions where the pumping

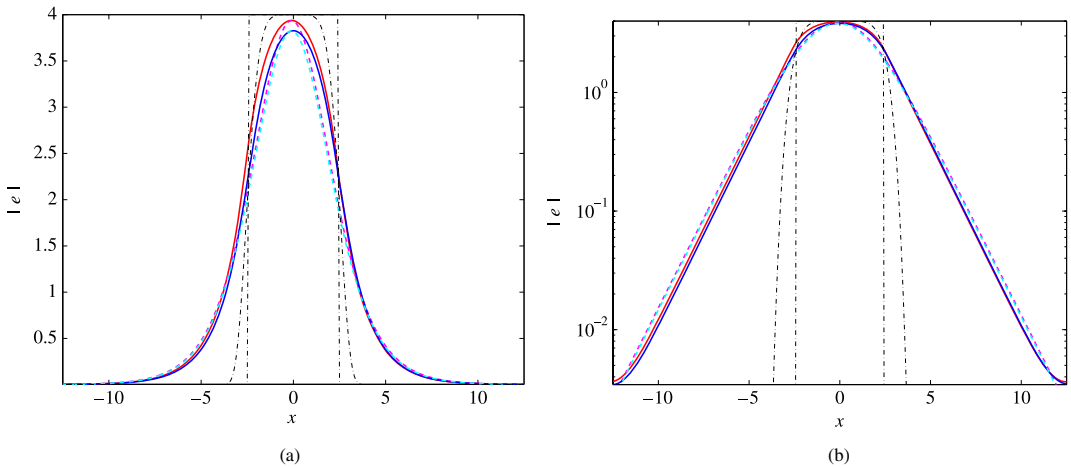


Figure 2. Transverse electric field amplitude profile in both linear (a) and logarithmic (b) scales. Solid curves: numerical resolution of the Maxwell–Bloch equations for super-Gaussian (upper, red curve) and top-hat (lower, blue curve). The dashed curves are sech^2 fits. The dash–dot curves are proportional to the top-hat and super-Gaussian pumpings.

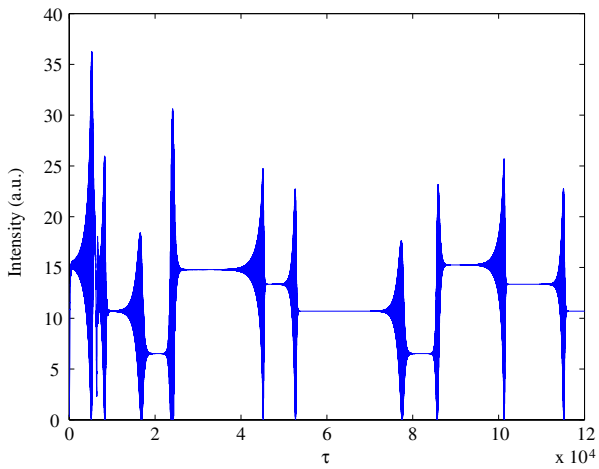


Figure 3. Time evolution of the intensity at a given position x, for a uniform pumping in a box with width 5, and periodic boundary conditions: intermittency.

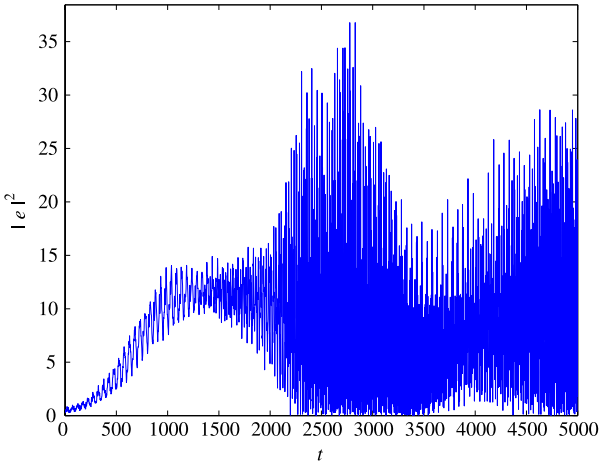


Figure 4. Time evolution of the intensity at $x = 0$, for a uniform pumping in a box with width 5, and reflecting boundary conditions: instability.

vanishes. The time evolution of the electric field envelope is a complex exponential with angular frequency $\Omega = 0.0246$. We can thus conclude that the presence of an inhomogeneous (a non-uniform) pumping profile leads to a stabilization of the laser space–time dynamics. Since the results obtained with the super-Gaussian and the top-hat pumping profiles are very close, we consider only the latter profile in the following analysis. We have further checked that this stabilization still occurs for other parameters in the instability parameter domain considered.

This stabilization would not be so surprising if the transverse dimension of the pumping profile corresponded to a low Fresnel number, as is the case in microchip lasers [12]. This is not the case, however, and the mechanism of this stabilization has to be explored. More precisely, the boundary conditions at the edge of the pumped zone play an important role in the stabilization process. This role must now be established. Complementary numerical simulations have thus been carried out: the previous results were first compared to those that were obtained considering a uniform pumping profile. Using a numerical box with the same width as the previous pumped zone (i.e. $2x_m$ with $x_m = 2.5$), we obtain the same type of intermittency as described in [11]; see figure 3. In conclusion, the reflection of the transverse waves on the edges of the pumped zone clearly plays a role in the stabilization, by inducing some stationary waves. In a second step, still considering a uniform pumping profile, but taking into account some reflection through the simple boundary conditions $e(x = \pm x_m) = 0$, or $\partial_x e(x = \pm x_m) = 0$, new numerical computations show that stable stationary waves do not exist in these conditions either. This is shown in figure 4, which presents the evolution of the intensity at $x = 0$ versus time, for a uniform pumping in a box with width 5, and assuming the previous simple reflecting boundary conditions. From these two comparisons, it appears clearly that the structure of the electric field outside the pumped zone is an essential part of the

stabilization process. To pursue our analysis, we have looked for stationary solutions to the Maxwell–Bloch equations, and particularly for evanescent wave fields in non-pumped regions.

3. Stationary solutions to the Maxwell–Bloch equations

3.1. The stationary equation

Let us now consider stationary states of the Maxwell–Bloch equations (1)–(3). Assuming that the electric field is stationary, $e = E(x)e^{i\Omega t}$, it is seen that the polarization has the same time dependence $p = P(x)e^{i\Omega t}$, with

$$P(x) = E + \frac{i}{\sigma}\left(\Omega E - A\partial_x^2 E\right), \tag{9}$$

and that the population inversion d is a constant, with

$$d = r - |E|^2 - \frac{A}{\sigma}\mathrm{Im}\left(E\partial_x^2 E\right). \tag{10}$$

Then, from equation (10) we get the equation satisfied by E, as

$$[1 + i(\Omega - \delta)]\left[1 + \frac{i}{\sigma}\left(\Omega - A\frac{\partial_x^2 E}{E}\right)\right] = r - |E|^2\left(1 + \frac{A}{\sigma}\mathrm{Im}\,\frac{\partial_x^2 E}{E}\right). \tag{11}$$

Equation (11) is split into real and imaginary parts, using

$$\frac{\partial_x^2 E}{E} = u + iv, \tag{12}$$

with u, v real. Then, setting

$$W = \frac{1}{\sigma}(\Omega - Au), \qquad \text{and} \qquad T = \frac{A}{\sigma}v + 1, \tag{13}$$

equation (11) can be written in the compact form

$$W = -(\Omega - \delta)T, \tag{14}$$

$$T = \frac{r}{1 + (\Omega - \delta)^2 + |E|^2}. \tag{15}$$

Computing back $(\partial_x^2 E)/E$ from equations (12) to (15), we get

$$(\Omega - i\sigma)E - A\partial_x^2 E + (\Omega - \delta + i)\sigma r \times \frac{E}{1 + (\Omega - \delta)^2 + |E|^2} = 0, \tag{16}$$

which is the general equation for the stationary states. It is of stationary saturated complex Ginzburg–Landau type.

3.2. A few analytical stationary-state solutions

Solutions to (16) with uniform $|E|$ are computed easily: the travelling wave solution (4)–(8) is retrieved. An evanescent wave solution is found assuming $E = \mathcal{E}e^{(-iK+\kappa)x}$. For a nonzero κ,

$$\frac{E}{1 + (\Omega - \delta)^2 + |E|^2} = \frac{\mathcal{E}e^{(-iK+\kappa)x}}{1 + (\Omega - \delta)^2 + |\mathcal{E}|^2 e^{-2\kappa x}}$$

is linearly independent of E, and hence this nonlinear term must vanish from the equation. Thus $r = 0$: the evanescent wave exists only where pumping is absent. Then we get

$$\kappa = \frac{\sigma}{2AK}, \tag{17}$$

$$\Omega = A\left(\kappa^2 - K^2\right). \tag{18}$$

Apart from the translation invariance in the x direction, this yields a one-parameter family of evanescent wave solutions.

For small values of x, and a nonzero pumping parameter r, a parabolic approximation of a solution can be given. We expand the electric field amplitude as $E = e_M t(1 + bx^2 + O(x^3))$, for a solution centred at $x = 0$. Substitution into equation (16) yields

$$b = \frac{\Omega - i\sigma}{2A} + (\Omega - \delta + i)\frac{\sigma}{2A}\frac{r}{1 + (\Omega - \delta)^2 + e_M^2}. \tag{19}$$

The linear chirp vanishes locally if

$$e_M^2 = r - 1 - (\Omega - \delta)^2, \tag{20}$$

which sets the maximum of E at the same value as the amplitude of the travelling waves. Then

$$b = \frac{\Omega}{2A} + (\Omega - \delta)\frac{\sigma}{2A}. \tag{21}$$

To sum up, different classes of stationary solution exist: the well-known travelling wave solution valid for homogeneous pumping, evanescent wave fields in domains where pumping vanishes, and also localized profiles, for which can be computed a parabolic approximation in the vicinity of the origin $x = 0$. The next section will show that the profile we observe is a combination of a parabolic-shaped field in the centre of the pumped region and of evanescent wave fields in the edges of the non-uniform pumping profile.

3.3. Comparison between analytical and numerical results

Let us detail the numerical results already presented in figure 2. A plot of the transverse profile of the field shows that it decays exponentially out of the pumped region, with a linear phase (cf figure 5). Hence the numerical steady state is correctly fitted by the evanescent wave in the non-pumped zone, as was assumed in the previous section. It is easily checked that for a given Ω, equations (17)–(18) admit only two opposite real solutions. The sign of κ is fixed by the direction of decrease, and thus determines the sign of K. Hence, for a given frequency Ω, there is only one possible evanescent wave in each direction. We check that the analytical solution coincides with the numerical results as follows: first the numerical data are fitted by straight lines (see figure 5), then we check that the value obtained satisfies relations (17)–(18). The fitting (a simple interpolation) yields $\Omega = 0.0246$, $K = \pm 0.1399$ and $\kappa = \pm 0.7145$. For this value of Ω, equations (17)–(18) give $K = \pm 0.1398$ and $\kappa = \pm 0.7152$. Hence, the field in the non-pumped region yields an evanescent wave, with $\Omega = 0.0246$.

Finally, let us consider the pumped region. In this domain, the transverse profile is well fitted by the chirp-free parabolic approximation (20)–(21), as can be seen in figure 6. The angular frequency of the electric field is $\Omega = 0.0246$.

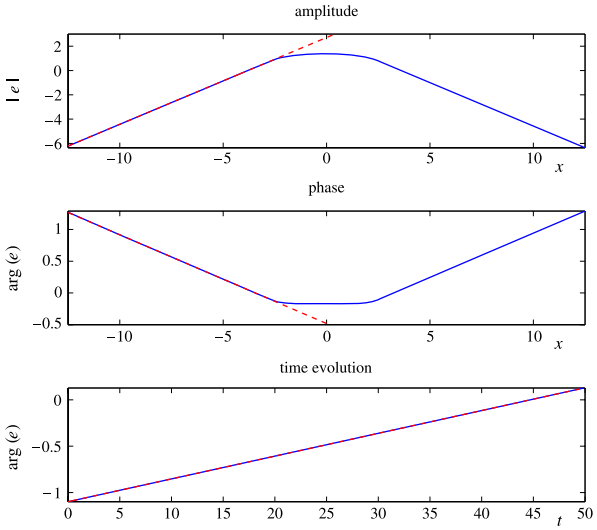


Figure 5. The field transverse profile ((a): logarithm of the amplitude, (b): phase), and (c) the time evolution of its phase in the non-pumped area. The dotted lines are the linear fitting.

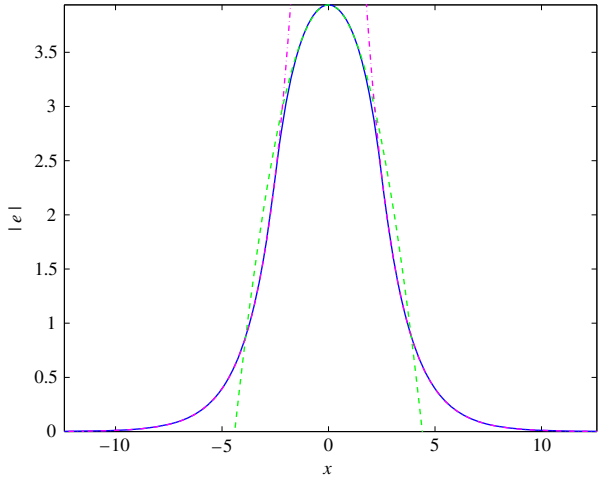


Figure 6. Fitting of the field transverse profile (solid blue line), using the evanescent wave solution (wings, dashed–dotted pink line) and the parabolic approximation (centre, dashed green line).

4. Linear stability and stabilization mechanism

4.1. Numerical computation and linear stability of the stationary states

For top-hat pumping, equation (16) can be solved by means of a shooting method. More precisely, we assume a symmetry with respect to the centre $x = 0$ of the pumped zone. Hence $\partial_x E$ is zero at this point. For arbitrary values of $E(x = 0)$ and Ω, the Cauchy problem for equation (16) is solved in the pumping zone. Then it must be matched to an evanescent wave solution in the non-pumped region, which yields the condition

$$\frac{\partial_x E}{E} = -\mathrm{i}K + \kappa, \tag{22}$$

where K and κ are functions of Ω, as defined by equations (17)–(18), to be satisfied at the boundary $x = x_m$. Taking the global phase invariance into account, this yields a set of two equations for the two variables $e_\mathrm{M} = |E(x = 0)|$ and Ω, which can be solved numerically. This scheme has been easily implemented using built-in functions of GNU Octave. The scheme fails to converge for values of r below a line in the (δ, r) plane, roughly between the points (2.5, 11) and (4, 18), which corresponds either to the first or to the second laser threshold. The steady state has a shape similar to the one given in figure 2 for a wide domain around the point $(\delta, r_0) = (3, 25)$ at which figure 2 was computed. For larger values of δ and r_0, the shape of the steady-state solutions changes radically. This is left for further study.

The stability of the stationary solutions has been investigated by numerically solving the Maxwell–Bloch equations linearized about the numerically computed stationary state. We used a standard fourth-order Runge–Kutta algorithm. The x-derivatives were computed by means of finite differences, and the initial data was a white noise. Since the decay is quite slow, computations were performed up to $t = 500$, and we needed to restrict the stability computation to a few points. The points investigated are indicated by crosses in figure 1. They were chosen close to the boundary of the domain limited by the threshold line mentioned above, the threshold of re-stabilization of the uniform solution for uniform pumping, the line $r = 80$, and the line $\delta = 4$ (see figure 1). Taking into account the limits of accuracy on Ω, all points were found to be stable. It can be reasonably conjectured that stability of the stationary state occurs in the entire domain.

Above the threshold of re-stabilization of the uniform solution for homogeneous pumping, the localized stationary solution still exists. This has been checked for $(\delta, r_0) = (2.6, 80)$ and is expected to hold over a wide range. However, this is of less interest, since the stability is ensured for uniform pumping in this case.

4.2. The transient evolution

Figure 7 shows the transient evolution of the transverse profile of the field during the stabilization. The evolution of the field profile can be summarized as follows: in a first stage, many travelling waves appear. They are reflected on the borders of the pumped zone. A stationary wave pattern develops, corresponding to the linear superposition of travelling waves whose wavelength λ matches the width l of the pumped zone, namely $\lambda/2 = l$, as in the formation of any linear standing wave. This can be shown by fitting the amplitude $|e(x)|$ with a cosine function having this wavelength, precisely $f_2(x) = (e_\mathrm{M} - e_\mathrm{m}) \cos \pi x/l + e_\mathrm{m}$, where e_M is the maximum value of $|e(x)|$, and e_m is the mean value in the non-pumped region (see figure 7, dashed light blue curves). Then, the amplitude of the standing wave grows, and its shape becomes modified by the nonlinear effect. When the amplitude, and hence the effect of nonlinearity, increases, the field profile separates from the linear standing wave mode, and its curvature decreases and becomes closer to that of the parabolic-shaped steady state. A fit with the parabola $f_2(x) = e_\mathrm{M}(1 + bx^2)$, where b has the value pertaining to the final steady state, given by

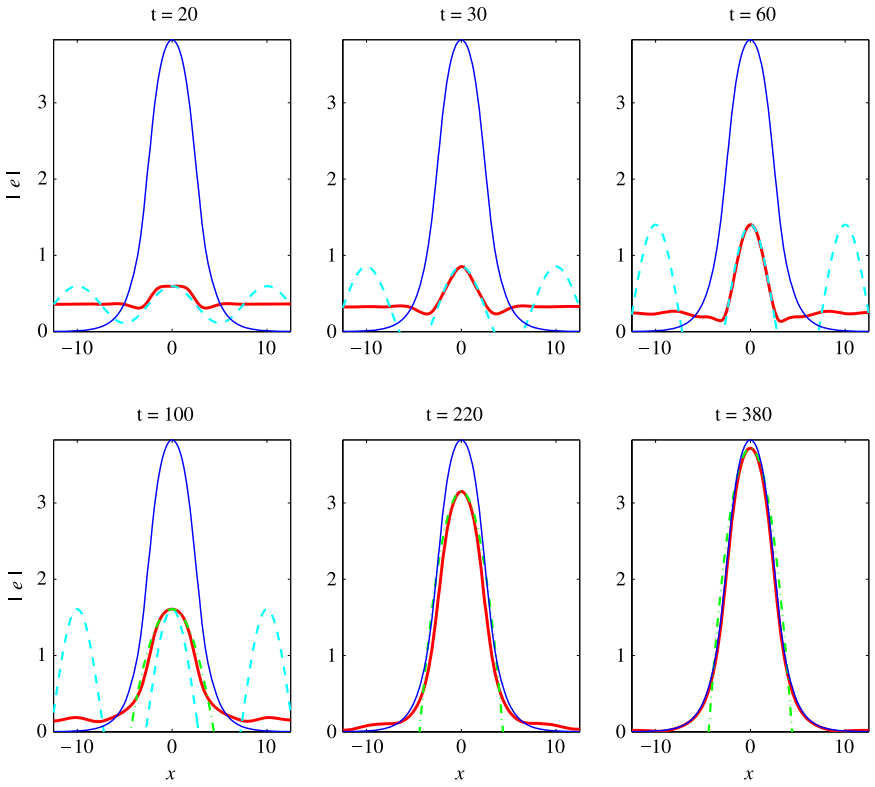


Figure 7. Transient evolution of the field transverse profile. Thick solid (red) line: evolution of the field profile. Thin solid (dark blue) line: final steady state. Dashed (light blue) line: fit with $e_{\mathrm{M}} \cos \pi x/l$. Dashed–dotted (green) line: parabolic approximation.

equation (21), is shown in figure 7 (bottom, dashed–dotted green curves).

Simultaneously, the profile in the non-pumped zone becomes close to the evanescent waves. This continues until the maximal amplitude corresponding to the exact steady state is reached. The latter is stable. As mentioned above, the angular frequency of the stable steady state is $\Omega = 0.0246$. Using the dispersion relation (8) of the travelling wave solutions (4)–(8) of the Maxwell–Bloch system, the corresponding wavenumber is $K = 0.321$. Hence $K \simeq (1/2)\pi/l = 0.314$. The selected frequency corresponds to the first subharmonic of the frequency matched with the size of the pumping box. The stabilization mechanism can thus be summarized as follows: the reflection of travelling waves on both edges of the pumping profile creates a stationary wave pattern which adapts itself to limit conditions (i.e. evanescent waves on both sides of the pumping profile, and a parabolic shape in its centre) through a subharmonic transition.

5. Conclusion

Let us first discuss how our theoretical predictions can be confirmed experimentally. Previous experimental works concerned semiconductor lasers in which the injection current profile was inhomogeneous [13] and CO_2 lasers where time resolved experiments were conducted [14]. In our case it is necessary to control the width of the pumping, and hence longitudinally pumped solid-state lasers should be used. The simplest laser configuration is a plane–plane microchip laser with one mirror directly deposited on the input face of the amplifying medium and a second bulk (output) mirror. A short cavity length of some hundreds of micrometers allows single-longitudinal laser oscillation and a slight translation of the output mirror permits control of the cavity detuning, which is of great importance in the transverse pattern formation. On the other hand, the size of the pumping beam has to be controlled and varied. Indeed, the laser must be first arranged to work in the unstable domain corresponding to positive detunings (cf figure 1). This is obtained with sufficiently large pump size and pumping level. If the pump size is then decreased, the transition from unstable operation (intermittency) to a stable stationary state must be observed by a suitable imaging of the near-field pattern emission in a CCD camera. Finally, our results can also be used as guidelines to design large-Fresnel-number stable laser sources by a suitable control of both the cavity detuning and the pump size.

The space–time dynamics of a homogeneously broadened single-mode laser (when diffraction is taken into account) has been studied under non-uniform pumping. We have considered both a super-Gaussian pumping profile and a top-hat one, which give very similar results. Our investigations reveal that unstable dynamics are stabilized in the presence of a non-uniform pumping. This stabilization is due to the creation of a stationary wave pattern exhibiting an evanescent profile on both sides of the pumped zone, and a parabolic shape in its centre. Stabilization occurs with a period doubling of the spatial pattern.

References

[1] Haken H 1975 Analogy between higher instabilities in fluids and lasers *Phys. Lett.* A **53** 77–8

[2] Tang D Y and Weiss C O 1994 Uniqueness of the chaotic attractor of a single-mode laser *Phys. Rev.* A **49** 1296–300

[3] Tang D Y, Heckenberg N R and Weiss C O 1995 The optical field of type-III intermittent pulsing of a single mode laser *Phys. Lett.* A **202** 363–8

[4] Lugiato L A and Milani H 1983 Disappearance of laser instabilities in a Gaussian cavity mode *Opt. Commun.* **46** 57–60

[5] Lugiato L A and Milani H 1985 Effects of Gaussian-beam averaging on laser instabilities *J. Opt. Soc. Am.* B **2** 15

[6] Louvergneaux E 2001 Pattern-dislocation-type dynamical instability in 1D optical feedback Kerr media with Gaussian transverse pumping *Phys. Rev. Lett.* **87** 244501

[7] Plumecoq J, Szwaj C, Derozier D, Lefranc M and Belawski S 2001 Eckhaus instability induced by nonuniformities in a laser *Phys. Rev.* A **64** 061801

[8] Jakobsen P K, Moloney J V, Newell A C and Indik R 1992 Space–time dynamics of wide-gain-section lasers *Phys. Rev.* A **45** 8129–37

[9] Jakobsen P K, Lega J, Feng Q, Staley M, Moloney J V and Newell A C 1994 Nonlinear transverse modes of large-aspect-ratio homogeneously broadened lasers: I. Analysis and numerical simulation *Phys. Rev.* A **49** 4189–200

[10] Lega J, Jakobsen P K, Moloney J V and Newell A C 1994 Nonlinear transverse modes of large-aspect-ratio homogeneously broadened lasers: II. Pattern analysis near and beyond threshold *Phys. Rev.* A **49** 4201–12

[11] Amroun D, Brunel M, Letellier C, Leblond H and Sanchez F 2005 Complex intermittent dynamics in large-aspect-ratio homogeneously broadened single-mode lasers *Physica* D **203** 185–97

[12] Sanchez F and Chardon A 1996 Transverse modes in microchip lasers *J. Opt. Soc. Am.* B **13** 2869–71

[13] Houlihan J, O'Callaghan J R, Voignier V, Huyet G and McInerney J G 2001 Experimental observation of travelling waves in the transverse section of a laser *Opt. Lett.* **26** 1556–8

[14] Encinas-Sanz F, Leyva I and Guerra J M 2000 Time resolved evolution in large aperture laser *Phys. Rev. Lett.* **84** 883–6